

Phase Transitions in a Probabilistic Cellular Automaton: Growth Kinetics and Critical Properties

F. J. Alexander,^{1,2} I. Edrei,^{1,3} P. L. Garrido,^{1,4} and J. L. Lebowitz¹

We investigate a discrete-time kinetic model without detailed balance which simulates the phase segregation of a quenched binary alloy. The model is a variation on the Rothman-Keller cellular automaton in which particles of type A (B) move toward domains of greater concentration of A (B). Modifications include a fully occupied lattice and the introduction of a temperature-like parameter which endows the system with a stochastic evolution. Using computer simulations, we examine domain growth kinetics in the two-dimensional model. For long times after a quench from disorder, we find that the average domain size $R(t) \sim t^{1/3}$, in agreement with the prediction of Lifshitz-Slyozov-Wagner theory. Using a variety of methods, we analyze the critical properties of the associated second-order transition. Our analysis indicates that this model does not fall within either the Ising or mean-field classes.

KEY WORDS: Probabilistic cellular automaton; domain growth kinetics; critical phenomena.

1. INTRODUCTION

When a uniform binary mixture is quenched from high temperature to a temperature at which the uniform state is no longer stable, it undergoes phase segregation. Concentration fluctuations, either long-wavelength, small-amplitude (spinodal decomposition) or small-wavelength, large-amplitude (nucleation), grow and form single-phase domains.^(1,2) If there are no external forces acting on the system, then the final state will be one

¹Departments of Physics and Mathematics, Rutgers University, Piscataway, New Jersey 08855.

²Present address: Center for Nonlinear Studies, Los Alamos National Laboratory, Los Alamos, New Mexico 87545.

³Present address: National Semiconductor, P.O. Box 619, Migdal Haemek, Israel.

⁴Present address: Dpto. Fisica Moderna Facultad de Ciencias, Universidad de Granada, Granada, Spain.

of phase coexistence in thermodynamic equilibrium. Of theoretical and practical interest is the domain growth kinetics and morphology following a quench in both of these cases.¹³

While phase segregation is a complicated nonlinear process, it is possible to build models with simple *microscopic* dynamics which give the correct and essential physics on the *macroscopic* level.¹⁴⁻⁹⁾ Kinetic Ising models have been among the most used in such investigations. These models evolve in continuous time according to a stochastic dynamics satisfying a detailed balance condition which guarantees that the stationary state is Gibbsian with respect to the Ising Hamiltonian.

The model investigated here is a discrete-time probabilistic cellular automaton (PCA) which, as we shall show, has some advantages over the Ising-type models. It is a variation on the model of Rothman and Keller (RK),⁽⁶⁾ who studied a lattice gas of the FHP (Frisch, Hasslacher, and Pomeau)⁽¹⁰⁾ type with two species of particles referred to as A and B. These particles evolve following an almost deterministic discrete-time dynamics, conserve momentum in collisions, and have a tendency to segregate by maximizing the local flux of A's and B's in the direction of their respective concentration gradients.

In our studies we introduce a stochastic element into the particle dynamics which mimics the effects of a thermal bath (characterized by an inverse temperature-type parameter β similar to ref. 8). Furthermore, we consider the situation where the total density of A's and B's is maximal. In this case, the momentum is locally identically zero, and can be effectively removed from the problem. This permits us to interpret one of the components as particles and the other as holes.⁽¹²⁾ Finally, we consider a square lattice model⁽¹¹⁾ rather than a hexagonal one for ease of simulations.

1.1. The Model

We consider a periodic $N \times N$ square lattice Γ having at each site $\mathbf{x} \in \Gamma$ as many as four particles. The global configuration η is described locally by $\eta(\mathbf{x})$, with Boolean components $\eta_{\hat{e}}(\mathbf{x})$, where $\hat{e} \in \{\pm \hat{e}_1, \pm \hat{e}_2\}$, the unit vectors along the lattice axes. $\eta_{\hat{e}}(\mathbf{x}) = 1$ represents the existence and $\eta_{\hat{e}}(\mathbf{x}) = 0$ the absence of a particle at the site \mathbf{x} with unit speed in the \hat{e} direction. The number of particles at site \mathbf{x} in configuration η is then given by

$$\eta(\mathbf{x}) = \sum_{\hat{e}} \eta_{\hat{e}}(\mathbf{x}) \quad (1)$$

and the number of holes by $4 - \eta(\mathbf{x})$. The particle flux vector at each site is

$$\mathbf{u}(\mathbf{x}; \eta) = \sum_{\hat{e}} \eta_{\hat{e}}(\mathbf{x}) \hat{e} \quad (2)$$

The system evolves in discrete time by a two-step dynamics with simultaneous updating at each node. These steps are propagation and collision. In propagation each particle moves one lattice unit in the direction of its velocity. Next, in collision, the particles at each site change their velocities according to a stochastic rule designed to facilitate particle-hole segregation.

Starting from η , we choose a new global configuration η' with probability

$$P(\eta'|\eta) = \prod_{\mathbf{x} \in \Gamma} \frac{1}{Z(\mathbf{x}; \eta, \eta')} \exp[\beta \mathbf{u}(\mathbf{x}; \eta') \cdot \mathbf{f}(\mathbf{x}; \eta)] \delta(\eta'(\mathbf{x}) - \eta(\mathbf{x})) \quad (3)$$

where

$$Z(\mathbf{x}; \eta, \eta') = \sum_{\eta'(\mathbf{x})} \exp[\beta \mathbf{u}(\mathbf{x}; \eta') \cdot \mathbf{f}(\mathbf{x}; \eta)] \delta(\eta'(\mathbf{x}) - \eta(\mathbf{x})) \quad (4)$$

is a normalization factor, and

$$\mathbf{f}(\mathbf{x}; \eta) = \sum_{\mathbf{y} \in \mathcal{A}_x} \eta(\mathbf{y}) \frac{(\mathbf{y} - \mathbf{x})}{|\mathbf{y} - \mathbf{x}|} \quad (5)$$

is the particle concentration gradient at \mathbf{x} computed in a neighborhood \mathcal{A}_x of "radius" r about each \mathbf{x} . For $r=1$, \mathcal{A}_x is just the set of nearest neighbor sites of \mathbf{x} . For $r=2$, \mathcal{A}_x extends to next-nearest neighbors, and so on. For $\beta > 0$ the rule (3)–(5) gives a preference for particle fluxes to be directed toward regions within \mathcal{A} with the highest particle density. The parameter β controls the degree of preference to maximize $\mathbf{u}(\mathbf{x}; \eta') \cdot \mathbf{f}(\mathbf{x}; \eta)$; at $\beta = 0$ all configurations consistent with local particle conservation have equal weight. At the other extreme, $\beta = \infty$ defines an almost deterministic model where $\mathbf{u}(\mathbf{x}; \eta') \cdot \mathbf{f}(\mathbf{x}; \eta')$ is *always* maximized. This is precisely the condition imposed in the Rothman and Keller model.⁽⁶⁾

Qualitatively, our dynamics is similar to that of a ferromagnetic Ising model with Kawasaki dynamics satisfying detailed balance with respect to a Gibbs measure. For $\beta \ll 1$ all collision outcomes (consistent with particle conservation) have approximately equal weights, while for large β , "favorable" outcomes occur with overwhelming probability. However, since our dynamics is not based on a Hamiltonian description with an interaction potential, we do not know the stationary measures of the system (for $\beta \neq 0$), and there is no reason to expect them to be Gibbsian with any finite range or rapidly decreasing interaction potential. We nevertheless refer to β^{-1} as the temperature, and to the stationary state as an equilibrium state, but this is meant only to be suggestive.

The model presented here is thus intermediate between the standard kinetic Ising models and the hydrodynamic cellular automata of Rothman *et al.*¹⁹⁾ We have used it in simulations as a means of enhancing the rate of segregation (compared to Ising models) without sacrificing temperature (common in CA simulations). It provides an alternate method by which to simulate ordering processes in quenched alloys. Here we focus attention on the kinetics of domain growth and an analysis of the static critical properties.

In Section 2 we describe the time evolution of our model, giving a quantitative description of the segregation kinetics. In particular, we find that the average size of the single-phase domains $R(t)$ follows, for times long after the quench, the Lifshitz–Slyozov–Wagner (LSW) growth law $R(t) \sim t^{1/3}$.^(2, 13) At low temperatures the dynamics gives rise to an anisotropic ordered phase. In Section 3 we explain the origin of this anisotropy and discuss the ergodic properties of this model. In Section 4 we study the properties of the critical point and of the two-phase region. Using a variety of techniques, we estimate the critical exponents. Finally, in Section 5 we investigate phase segregation in this model when a driving field induces a particle flux in a preferred direction.

2. KINETICS

A system with $4\rho N^2$ particles on T , $0 < \rho < 1$, was put in an initial disordered state typical of a system at $\beta = 0$, i.e., particles randomly distributed over the lattice sites. We then studied its evolution under the dynamics with some $\beta > \beta_c \approx 0.32$ —the critical value determined by a number of simulation methods given later—where we know that its final stationary state is segregated, resembling a coexistence of two phases. The results depended on the values of β , the concentration ρ , the interaction range r , and the lattice size N .

Here we concentrate on $r = 1$ and $\rho = \frac{1}{2}$ for ease of comparison with the known behavior of nearest neighbor Ising systems. We also restrict ourselves to $N = 128$, where the finite-size effects on the dynamics of phase separation appear to be small at the values of β considered.

We show in Fig. 1 a typical sequence of domain configurations in the evolution of the model for various times after a quench from disorder. The



Fig. 1. Typical sequence of configurations following a quench from disorder.

particle density is $\rho = \frac{1}{2}$ and inverse temperature $\beta = 0.625$. The density of particles at a site is proportional to its darkness. As is visually evident, single-phase domains form and grow as the impurities within those regions decrease.

The time evolution of segregation processes in physical systems is often monitored experimentally through the spectrum of scattered radiation. This is directly related to the structure function $S(\mathbf{k}, t)$, the Fourier transform of the density-density correlation function^(12, 15):

$$S(\mathbf{k}, t) = \frac{1}{|T|} \left\langle \sum_{\mathbf{x} \in T} e^{i\mathbf{k} \cdot \mathbf{x}} \left[\frac{1}{4} \eta(\mathbf{x}) - \rho \right]^2 \right\rangle \quad (6)$$

where the angle brackets $\langle \cdot \rangle$ signify an ensemble average. In computer simulations this average is realized by collecting data from several independent runs. The extent of segregation is then determined by the location and intensity of the peak in the structure function. As the system segregates, the peak moves to smaller values of $|\mathbf{k}|$, and $S(\mathbf{k}, t)$ narrows while increasing in amplitude.⁽¹⁵⁾

Although information concerning anisotropy is lost in the integration, it is useful to average the structure function $S(\mathbf{k}, t)$ over shells of radius k . In a wide variety of phase-segregating systems this circularly averaged structure function has been observed to follow a scaling relation at late times:

$$S(k, t) \approx S(k_{\max}(t), t) F\left(\frac{k}{k_{\max}}\right) \quad (7)$$

where k_{\max} is the wavevector k at which $S(k, t)$ has its maximum at time t . These scaling functions for $\beta^{-1} = 1.6$ are shown in Fig. 2. The superposi-

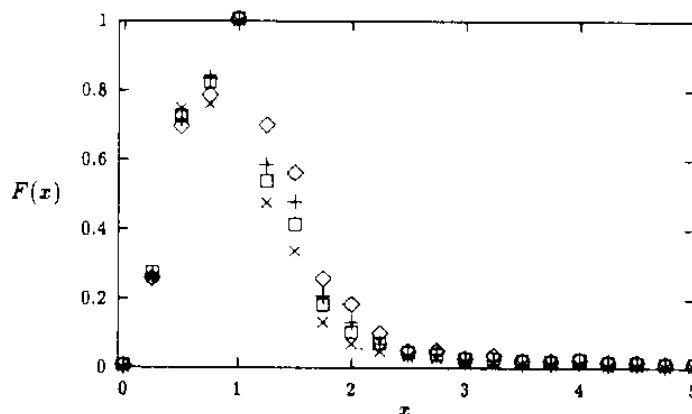


Fig. 2. Scaling function $F(x)$ for various times: (◇) 70000, (+) 80000, (□) 90000, and (×) 100000 steps.



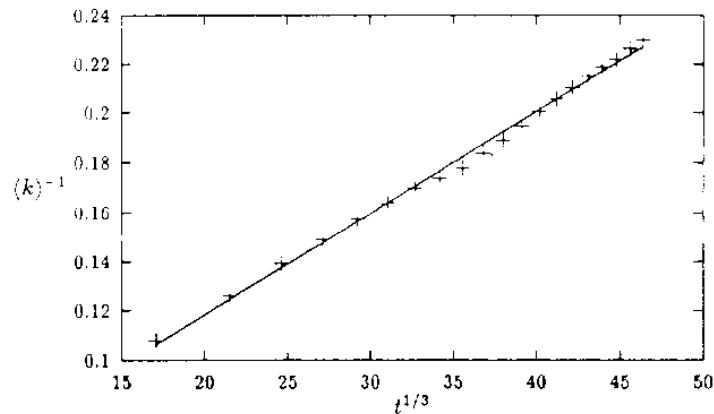


Fig. 3. The time evolution of the average domain size characterized through $\langle k \rangle^{-1}$ for $\beta = 0.625$.

tion is very good for large and small x , but there is a region $1 < x < 3$ where there are deviations from superposition. This may be due to the small number of independent runs we averaged.

Using the structure function computed before as a weight, we can get the average wavevector $\langle k(t) \rangle$, which will characterize the average domain size through $R(t) \sim \langle k(t) \rangle^{-1}$. We have

$$\langle k(t) \rangle \equiv \frac{\sum_k k S(k, t)}{\sum_k S(k, t)} \quad (8)$$

The data are presented in Fig. 3. This behavior is consistent with the LSW theory of phase domain growth for systems with conserved density.⁽²⁾ Note, however, that in our model the asymptotic regime appears earlier (fewer site updates) than in traditional Ising simulations.⁽¹³⁾

3. ANISOTROPY AND ERGODIC BEHAVIOR

As is clear in the snapshots of the segregated systems shown in Fig. 1, there is a predominant alignment of interfaces diagonal to the lattice axes. To understand this, we compare the stability at $\beta \gg 1$ of an interface oriented parallel to the lattice axes (Fig. 4a) with one where it is diagonal (Fig. 4b). At $\beta = \infty$ the state with the largest weight, as given by Eqs. (3)–(5), will *always* be selected in the collision step. Hence both of these configurations will be stationary. For $\beta < \infty$, however, all possible states will be sampled. There is then a small but nonzero probability that a flux will be chosen, which will after the interface at the next propagation step.

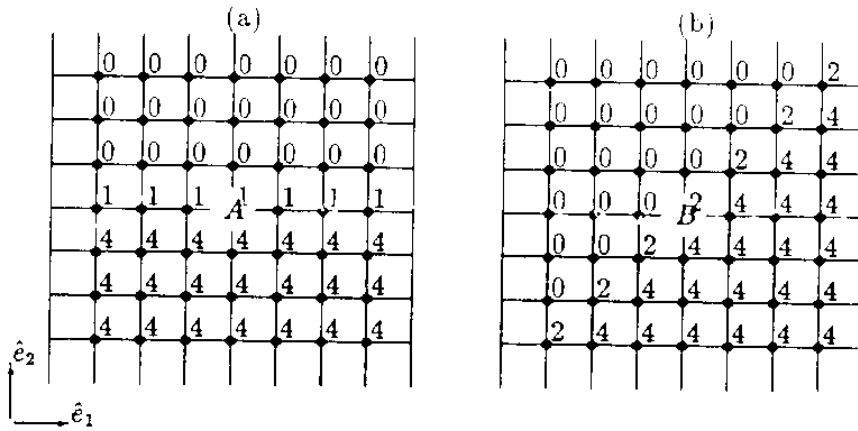


Fig. 4. Stable configurations at $\beta = \infty$. The number associated with each site indicates the number of particles at each site.

Given a particular site on the interface, we calculate the probability that such a defect will occur at that site in a given time step. For large β , this will be determined primarily by the ratio of the weight of the most likely defect to the weight of the interface-preserving choice.

We carry out the calculation for $r = 1$. Consider the flat interface in Fig. 4a. The only place a defect can occur during the collision step is at a site occupied by one particle. Choose such a site and label it A . The particle concentration gradient at A is $\mathbf{f}(A) = -4\hat{e}_2$, since the 1-direction component vanishes. The interface-preserving collision has $\mathbf{u}(A) = -\hat{e}_2$, with weight $W \sim \exp(\mathbf{u} \cdot \mathbf{f}) = \exp(4\beta)$. The most likely defect will occur with the single particle having a velocity parallel to the interface. This yields $W \sim \exp(\pm \hat{e}_1 \cdot \mathbf{f}) = 1$. The rate at which a defect occurs is then approximately $\exp(-4\beta)$.

For a diagonal interface defects only occur at the sites on the interface with two particles. Choose one and label it B . The particle concentration gradient is $\mathbf{f}(B) = 4(\hat{e}_1 - \hat{e}_2)$. The collision which preserves the interface will place the particles in the \hat{e}_1 and $-\hat{e}_2$ velocity directions, which gives $W \sim \exp(8\beta)$. The most probable defect will occur when one particle is put in a velocity mode aimed at the interface: either \hat{e}_1 or $-\hat{e}_2$; the other is placed in the opposite direction. This gives $\mathbf{u}(B; \eta') = 0$ and a weight $W \sim 1$. Defects then occur at a rate $\sim \exp(-8\beta)$. As $\exp(-8\beta) \ll \exp(-4\beta)$ for $\beta \gg 1$, we are led to believe that for $r = 1$ diagonal interfaces are more stable.

We can generalize these calculations to larger r , finding that for a horizontal (vertical) interface, defects occur at a rate

$$\text{Rate(Horizontal)} \sim \exp \left[-4\beta \sum_{|i|+|j| \leq r, i+j > 0} \frac{(i+j)}{(i^2+j^2)^{1/2}} \right] \quad (9)$$

For a diagonal interface, however, we have that

$$\text{Rate(Diagonal)} \sim \exp \left[-4\beta \sum_{r+i \leq r, j > 0} \frac{i}{(i^2 + j^2)^{1/2}} \right] \quad (10)$$

On the basis of this we conclude that diagonal interfaces are more stable than ones aligned with the lattice axes, for arbitrary choice of r . We observe that the anisotropy and flatness of interfaces is pronounced even at temperatures not too far below criticality.

3.1. Ergodic Behavior

In this section we prove that the final stationary state of this model is unique except for one spurious conservation law which we now explain. The lattice splits into two sublattices, odd and even, such that the particles on the odd (even) sublattice at odd time steps are the same particles which are on the even (odd) sublattice at even times. This is a result of the deterministic propagation step alone and has nothing to do with random collisions. There are thus always two ergodic components. For large enough systems and a random deposition of particles and holes, it is highly improbable that there will be a large difference between the densities of the two sublattices, and so we do not consider this further.

We want to show that the system will sample all possible states with a fixed sublattice occupation (for any density $\rho < 1$). To prove this, it is sufficient to show that all configurations with a specified number of particles on each sublattice can evolve into *one* particular configuration. Then, since it is possible for $\beta \neq \infty$ to retrace any step in the dynamics, they can evolve into each other. Ergodicity then follows from general results of finite-state Markov processes.

Let us consider the Q particles which are on the even sublattice at time $t=0$. We label these particles $1, 2, \dots, Q$ and assign to each of them a "target" site on the even sublattice and a "target" velocity mode at that site. These assigned sites are such that the lattice is filled up row by row starting from the site at the lower left corner, which will contain particles $1, \dots, 4$. Once the even sublattice sites of a row are filled, we move on to the next even row.

Each site will contain its maximum of four particles, with the final site possibly containing less. The velocity modes which each particle will occupy are determined by rotations of $\pi/2$ counterclockwise about the origin.

Our goal is to show that at some finite, even time step in the future we can find all of these particles at their designated locations. Thus, we

must show that there is a nonzero probability of this occurring. This is accomplished by first restricting all particles, except particle 1, to a back-and-forth motion (oscillating between their site at time zero and the site in the direction of their $t=0$ velocity). The first particle is then artificially moved to its designated site along some path by always selecting the collision rule which will accomplish this. If it encounters other particles, then it is given preference in any collision step so that it finds the correct mode. When it arrives at its designated site, we then lock it into the "back-and-forth" motion and move on to particle 2. Each step involved has nonzero probability, since β is finite. Therefore, the entire process has a nonzero (albeit very small) probability of occurring, and we are done.

4. CRITICAL BEHAVIOR

The analysis and characterization of critical behavior in non-Gibbsian particle models is difficult. When the dynamics is conservative (particle number remains constant), it becomes even more problematic: we have particle conservation, and cannot use the globally averaged particle density as the order parameter. Two alternatives are available. Instead of considering the *global* average of the particle density ρ , we may study the probability distribution of densities in subblocks of the entire system. Particles will be transferred between these subblocks via diffusion, and in this sense the conservation law can be "avoided." Of interest is the statistics of densities within these blocks. The other option is to define an order parameter which reflects the morphology (boundaries and internal structure) of the single-phase domains. We will use both methods as well as the behavior of a short-range order parameter to obtain information about the critical behavior of our model.

4.1. Block Distribution Functions

The block spin distribution method outlined here was pioneered by Binder and has since been used successfully for a variety of different models, including XY models, Potts models, and polymers.⁽²⁰⁻²²⁾ While the method was originally applied to Ising models without a conservation law, Binder has pointed out that it is applicable to conservative systems, provided the largest block size considered is much smaller than the overall lattice.⁽²²⁾ For convenience we rescale the site occupation variable η in our model to resemble the local spin in the Ising model:

$$S(\mathbf{x}) = \frac{\eta(\mathbf{x}) - 2}{4} \quad (11)$$

and hereafter refer to the local variables $S(\mathbf{x})$ as spins.

Partitioning the $N \times N$ lattice into blocks each of size $L \times L$, we define the spin of block i to be

$$s_i = \frac{1}{L^2} \sum_{\mathbf{x} \in \text{ith cell}} S(\mathbf{x}) \quad (12)$$

For each size L we then determine the probability distribution for the rescaled spins of that size block, $P_L(s)$. Because of the symmetry between particles and holes at density $\rho = 0.5$, we have

$$P_L(s) = P_L(-s) \quad (13)$$

For $T > T_c$, these distributions are expected to approach in the limit $L \rightarrow \infty$, taken after the limit $N \rightarrow \infty$, a Gaussian with mean zero,⁽²⁰⁻²²⁾

$$P_L(s) \rightarrow L(2\pi k_B T \chi_L)^{-1/2} \exp\left(\frac{-s^2 L^2}{2\pi k_B T \chi_L}\right) \quad (14)$$

where χ_L is a susceptibility. Conversely, for $T < T_c$, these distributions should tend toward two Gaussians centered at $\pm m$, the spontaneous magnetization of the infinite lattice. We have

$$P_L(s) \rightarrow \frac{L}{2} (2\pi k_B T \chi_L)^{-1/2} \left\{ \exp\left[\frac{-(s-m)^2 L^2}{2\pi k_B T \chi_L}\right] + \exp\left[\frac{-(s+m)^2 L^2}{2\pi k_B T \chi_L}\right] \right\} \quad (15)$$

This description is valid only in the region near $s = \pm m$. As a result of phase coexistence, the tails of the two terms near $|s| = 0$ deviate considerably from Gaussian. In any case, we expect that when $T < T_c$, one can determine m by measuring for large L any of the following quantities:

$$m_L \simeq \langle |s| \rangle_L \simeq \langle s^2 \rangle_L^{1/2} \simeq m \quad (16)$$

4.2. Simulation of Block Distributions

As seen from the pictures of the segregation process (Fig. 1), it takes the system more than 10^5 time steps to get into a stationary state at low temperatures, when the initial configuration is disordered. We avoid this difficulty by working in reverse and heating a completely ordered system, rather than quenching a disordered one. Metastability and hysteresis do not seem to be a problem here, as we have tested heating and cooling for several temperature and found that they tend to the same stationary state.

On a 128×128 lattice with particle density $\rho = 0.5$, the particles are initially configured in a compact, diamond-shaped domain. We then heat

the system to temperature $T=2$ and allow it to reach a stationary state. Stationarity is determined by monitoring quantities like the "surface area" (energy) E and average wavenumber $\langle k(t) \rangle$ and checking for Gaussian behavior in the statistics of these variables. After the system "equilibrated" at that temperature, we carried out the following program: We partitioned the system into subblocks of size $L \times L$, where $L = 1, 2, 4, 8,$ and 16 . At specific time intervals (usually 10-50 time steps), we recorded the net spin within the blocks. In our simulations it was computationally efficient to record the moments $\langle s_L^k \rangle$ of the distribution function $P(s)$ rather than $P(s)$ itself,

$$\langle s_L^k \rangle = \int ds s^k P_L(s), \quad k = 2, 4 \quad (17)$$

After recording the data, we increased the temperature slightly and then allowed for reequilibration. We call this approach Method I. Typically, this method has been applied to systems with nonconserved magnetizations.

To avoid the problems inherent in the restriction that L be small compared to N , we also carried out a block spin analysis of the region deep within one of the segregated domains. This method avoids the conservation problems and has the advantage that we could confidently look at blocks up to size 16 and perform a better extrapolation [Eq. (16)] for the order parameter. The drawback is that there were fewer blocks, and so the statistics was not as good. We call this approach Method II.

We present in Fig. 5 the order parameter determined by Method II using various sizes L . The results are consistent with those obtained by Method I. In the critical region we expect that this order parameter takes the form

$$m \sim \left(1 - \frac{T}{T_c}\right)^\beta \quad (18)$$

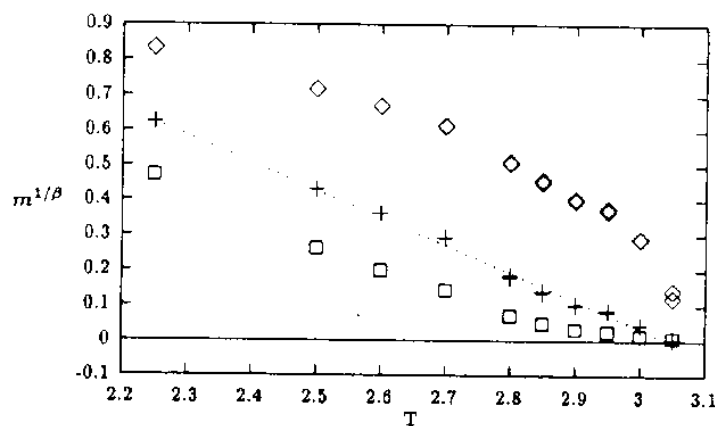


Fig. 5. Order parameter (Method II): $\beta = (\diamond) \frac{1}{2}$, $(+)$ 0.20, and $(\square) \frac{1}{4}$.

where β is the order parameter critical exponent. By plotting $m^{1/\beta}$ against temperature for different values of β , we can estimate the order parameter critical exponent to be the β which gives the best fit to a straight line. On the basis of this we find that $\beta \approx 0.20$. For comparison we also plot m^8 and m^2 . These correspond to the two-dimensional Ising model critical exponent $\beta = \frac{1}{8}$ and the exponent $\beta = \frac{1}{2}$.

From this analysis it appears that our model does not fall into either universality class, but we cannot rule out a crossover to $\beta = \frac{1}{2}$ or Ising behavior closer to the critical temperature. In Section 4.3 we will offer a similar analysis of the morphological order parameter and compare the results.

As noted in Eqs. (14) and (15), the block-spin distribution function above criticality will be a Gaussian, while below T_c , there will be two distinct peaks. A good indication of the Gaussian character of a distribution $P_L(\cdot)$ is

$$U_L = 1 - \frac{\langle s_L^4 \rangle}{3\langle s_L^2 \rangle^2} \quad (19)$$

which vanishes for a Gaussian distribution and has the value $\frac{2}{3}$ for a sharply peaked bimodal distribution. We examine whether, as L increases, the distribution becomes more Gaussian-like, with $U_L \rightarrow 0$, in which case we assume that we are in the one-phase region $T > T_c$. If, on the other hand, $U_L \rightarrow \frac{2}{3}$ with increasing L , then we assume that $T < T_c$. At the critical temperature, U_L should not depend on L , since on all scales the block spin distribution function will have the same character.

This makes the block spin analysis of critical phenomena possible without any previous knowledge of the magnitude of the correlation length. Furthermore, it provides a means by which to estimate the critical temperature and critical exponents independently of each other. We have examined U_L with both methods I and II and indicate the results for II in Fig. 6. For $T > 3.10$ there are no segregated regions, U_L tends to zero, and both methods give almost identical results. For $T \leq 3.05$, the cumulant tends to $\frac{2}{3}$. We thus conclude that T_c lies between 3.05 and 3.10.

For a system of subblocks, Binder has shown that one may estimate the correlation length exponent ν and the specific heat exponent α by plotting U_{bL} (b is a rescaling factor) versus U_L and determining the slope at T_c . The results for Method II are given in Fig. 7. We have

$$\left. \frac{\partial U_{bL}}{\partial U_L} \right|_{T_c} \approx b^{(1-\alpha)\nu} \quad (20)$$

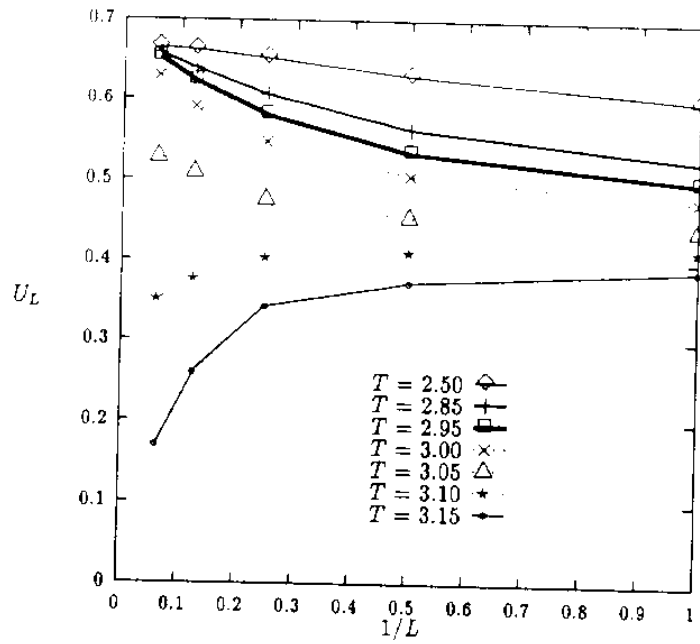


Fig. 6. U_L vs. $1/L$: Method II.

Both methods indicate that

$$\left. \frac{\partial U_{bL}}{\partial U_L} \right|_{3.05, 3.10} \approx 1.46 - 1.50 \quad (21)$$

for $b = 2, 4$. This is apparently insensitive to the exact location of T_c . Thus, we find that

$$\frac{1 - \alpha}{\nu} \approx 0.58 - 0.55 \quad (22)$$

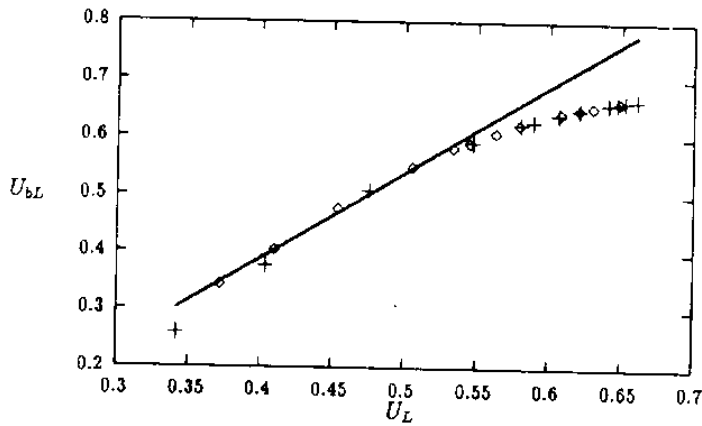


Fig. 7. U_{bL} vs. U_L : Method II.

As a result of the scaling of the distribution function at criticality, one also has the estimate

$$\frac{-\log(\langle s^2 \rangle_{hL} / \langle s^2 \rangle_{L,1})}{\log h} \approx \frac{2\beta}{\nu} \quad (23)$$

We find from method II, using $T_c = 3.05$, that

$$2\beta/\nu \approx 0.35-0.36 \quad (24)$$

This, in conjunction with our previous results by method II, gives an estimate $\nu \approx 1.1$ and so $0.36 < \alpha < 0.40$.

4.2.1. A Related Model. Chan and Liang⁽⁸⁾ have recently studied the static critical behavior for a related hexagonal lattice model. Instead of maximal occupancy, their model contains particles of two types, A and B, in addition to holes. Thus, momentum conservation plays a key role in determining the possible outcomes of collisions.

Chan and Liang's analysis, however, consisted of looking at the block spin distribution functions only for one small block size. Specifically, they considered $P(s)$ for a set of sites consisting of one site and four of its six nearest neighbors. They calculated the distributions $P(s)$ for a number of different temperatures, and stated that the critical temperature was the temperature at which the distribution was no longer Gaussian (single-peaked) in shape. What they neglected to do was to consider large L , while having $L \ll N$. Even above the critical temperature, the correlation length will be larger than one or two lattice sites and so one would expect that the distribution will not be Gaussian.

For a comparison of models, we carried out an analysis similar to theirs for our model and actually got similar results for the purported order parameter exponent, $\beta \approx 0.3$. Without actually modeling the identical system, it is impossible to say whether or not the exponents they quote are correct or not, but we believe that the method, as they have presented it, is incorrect.

4.3. Morphological Order Parameter

Visual examination of system configurations at low temperatures in the stationary state achieved at late times after a quench indicates that the system is nonuniform. Since we are in a nonequilibrium situation, we cannot rely on some thermodynamic principle to characterize the stationary state distribution of domain interfaces, such as minimization of the free energy. We nevertheless follow a prescription given by Binder and Wang

for calculating an order parameter based solely on the geometry of the low-temperature phase.⁽²³⁾ This assumes that the number of interfaces will be minimized and thus that one has some knowledge of how the low-temperature phase will manifest itself. Their order parameter consists of Fourier transforms of the spin configuration projected onto the individual lattice axes. The individual order parameters are Ψ_1^{\sin} , Ψ_1^{\cos} , Ψ_2^{\sin} , and Ψ_2^{\cos} , and are defined by

$$\Psi_1^{\sin} = \sum_{x=1}^N \sum_{y=1}^N S(x, y) \sin\left(\frac{2\pi}{n} y\right) \quad (25)$$

$$\Psi_1^{\cos} = \sum_{x=1}^N \sum_{y=1}^N S(x, y) \cos\left(\frac{2\pi}{n} y\right) \quad (26)$$

$$\Psi_2^{\sin} = \sum_{x=1}^N \sum_{y=1}^N S(x, y) \sin\left(\frac{2\pi}{n} x\right) \quad (27)$$

$$\Psi_2^{\cos} = \sum_{x=1}^N \sum_{y=1}^N S(x, y) \cos\left(\frac{2\pi}{n} x\right) \quad (28)$$

where the x axis corresponds to the 1-axis, the y axis corresponds to the 2-axis, and $S(x, y)$ is the density-density correlation function in the stationary state. For periodic boundary conditions the interfaces can occur anywhere, and so the individual order parameters are realization-dependent. We eliminate this dependence by forming a "mean-square" order parameter out of the individual order parameters,

$$\Psi^2 = (\Psi_1^{\sin})^2 + (\Psi_1^{\cos})^2 + (\Psi_2^{\sin})^2 + (\Psi_2^{\cos})^2 \quad (29)$$

Expecting that this order parameter follows the same scaling behavior as in Eq. (18) (for method II), we determine its values for large N and plot Ψ

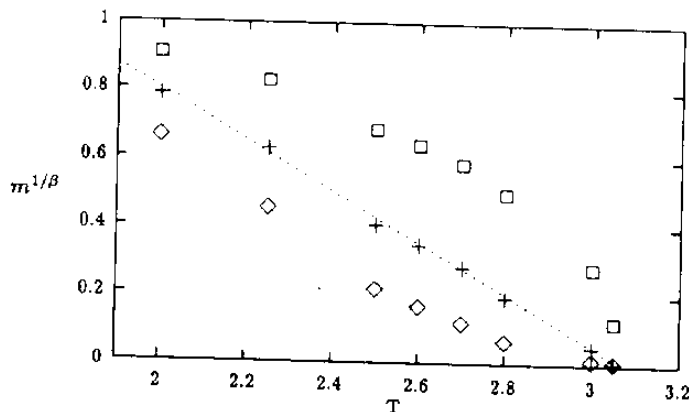


Fig. 8. Morphological order parameter $m^{1/\beta}$ for $\beta = (\square) \frac{1}{2}$, $(+)$ 0.22, and $(\diamond) \frac{1}{8}$.

raised to the various powers corresponding to mean-field and two-dimensional Ising model exponents. We find (Fig. 8) that the exponent which describes these data over the range $2.0 \leq T \leq 3.05$ is $\beta \approx 0.22$. This is consistent with the previous result obtained from Method II.

4.4. Short-Range Order Parameter

Recently, Marro *et al.* have analyzed the critical properties of a number of lattice models by using a short-range order parameter.⁽¹⁸⁾ The utility of this method is that it can give a qualitative indication of the universality class of a phase transition almost by visual inspection. These order parameters exhibit different qualitative features for different types of critical behavior. The order parameter σ is defined by

$$\sigma \equiv (1 - e)^{-2} \left[\frac{1}{4}(1 + e)^2 - m^2 \right] \quad (30)$$

where e is a nearest neighbor "energy"

$$e \equiv -\frac{1}{|F|} \sum_{\langle xy \rangle} \frac{1}{4} [\eta(\mathbf{x}) - 2][\eta(\mathbf{y}) - 2] \quad (31)$$

with summation over nearest neighbor pairs, and m is a long-range order parameter such as the ones we have calculated previously. Near the critical point (T_c), σ is expected to have the form

$$\sigma = \sigma_c + a_1 \varepsilon^{1-\alpha} - a_2 \varepsilon^{2\beta} \quad (32)$$

and $\varepsilon = 1 - T/T_c$ and the coefficients are nonsingular. For $\alpha = 0$ and $\beta = \frac{1}{2}$ there is no singularity at T_c , and σ decreases monotonically as a function of T . For nonclassical behavior ($\beta \neq \frac{1}{2}$), σ develops a maximum at T_c . Application of the method to our case, using the magnetization given by Method II, indicates that the behavior probably does not correspond to the mean field value $\beta = \frac{1}{2}$.

5. FIELD-DRIVEN MODEL

In addition to phase segregation and critical behavior in "equilibrium" systems, there is also a great deal of interest in these topics as they pertain to strongly nonequilibrium systems. Here we present of the features of a driven version of the model outlined above.

We modify the dynamics given by Eqs. (3)–(5) by including a field \mathbf{F} which induces a particle current parallel to \mathbf{F} :

$$P(\eta' | \eta) = \prod_{x \in F} \frac{1}{Z(x; \eta, \eta')} \exp[\beta \mathbf{u}(x; \eta') \cdot \mathbf{f}(x; \eta) + \mathbf{u}(x; \eta') \cdot \mathbf{F}] \delta(\eta'(x) - \eta(x)) \quad (33)$$



Fig. 9. Typical configurations for $|\mathbf{F}| = 4$ and (left to right) $T = 1.2, 1.5,$ and 1.6

where now

$$Z(x; \eta, \eta') = \sum_{\eta(x)} \exp[\beta \mathbf{u}(x; \eta') \cdot \mathbf{f}(x; \eta) + \mathbf{u}(x; \eta') \cdot \mathbf{F}] \delta(\eta'(x) - \eta(x)) \quad (34)$$

Our analysis consists of simulations for different temperatures on a 128×128 lattice and $|\mathbf{F}| = 4$. Without attempting a precise characterization of the critical phenomena, we do observe a number of interesting properties. First, the transition to a striped phase in Fig. 9 (the traditional ferromagnetic DDS transition) occurs (for these particular parameters) at a temperature below $T_c(\mathbf{F} = 0)$. This contrasts with the results for the two-dimensional KLS model, where $T_c(\mathbf{F} \neq 0) \approx 1.3T_c(\mathbf{F} = 0)$. There also appears to be a second transition at a lower temperature to a phase with structures resembling those found for $\mathbf{F} = 0$ (Fig. 9).

By using a morphological order parameter similar to the one described above, we find that the critical temperature $T_c(|\mathbf{F}| = 4) \approx 1.65$. The best fit of this order parameter to various powers $m^{1/\beta}$ occurs for $\beta \approx 0.5$. This result is, however, only preliminary. Further analysis needs to be performed.

6. DISCUSSION

We have presented a new stochastic cellular automaton in order to simulate phase segregation in binary mixtures. A temperature-like parameter gives us control on the depth of the quench and thus the degree of segregation.

We note that one of the complaints registered against Kawasaki exchange dynamics in Ising simulations is that the motion is too restrictive.⁽⁵⁾ There is no easy exchange of particles and holes at low temperatures, and this leads to an apparent reduced growth exponent and has hampered the analysis of late-stage domain growth. In the past, analyses of such behavior in Ising models have relied on extrapolation schemes⁽¹³⁾ or concluded that the growth exponent is less than $\frac{1}{3}$. The freedom of movement in the propagation step may be helpful in overcoming such problems, and with relative ease of computation we recover the predicted long-time growth behavior. In the same way, we seem to be bothered less by metastability effects than in standard Kawasaki dynamics.

It is interesting to note that our critical exponent β is in close agreement with β measured in two-dimensional simulations of a randomly driven diffusive system.⁽²⁵⁾ These models essentially involve an infinite temperature exchange along one the lattice axes and a finite temperature exchange along the other. It would be interesting to understand if and how these models are related.

ACKNOWLEDGMENTS

We would like to thank Z. Cheng, G. Eyink, D. Huse, S. Janowsky, H. Jauslin, J. Marro, D. Rothman, and S. Zaleski for useful comments and suggestions. This work was carried out using the computational resources of the Northeast Parallel Architecture Center (NPAC) at Syracuse University. This work was supported in part by NSF grant DMS89-18903. F. J. A. was supported in part by a Rutgers University Excellence Fellowship and in part by the Department of Energy at Los Alamos National Laboratory.

REFERENCES

1. H. Furukawa, *Adv. Phys.* **34**:703 (1985).
2. J. D. Gunton, M. San Miguel, and P. S. Sahni, in *Phase Transitions and Critical Phenomena*, C. Domb and J. L. Lebowitz, eds. (Academic Press, New York, 1983).
3. P. Fratzi, J. L. Lebowitz, O. Penrose, and J. Amar, *Phys. Rev. B* **44**:4794 (1991).
4. J. L. Lebowitz, E. Presutti, and H. Spohn, *J. Stat. Phys.* **51**:841 (1988).
5. Y. Oono and S. Puri, *Phys. Rev. A* **38**:434 (1987).
6. D. H. Rothman and J. M. Keller, *J. Stat. Phys.* **52**:1119 (1988).
7. C. Appert and S. Zaleski, *Phys. Rev. Lett.* **64**:1 (1990).
8. C. K. Chan and N. Y. Liang, *Europhys. Lett.* **13**:495 (1990).
9. H. Chen, S. Chen, G. D. Doolen, Y. C. Lee, and H. A. Rose, *Phys. Rev. A* **40**:2850 (1989).
10. U. Frisch, B. Hasslacher, and Y. Pomeau, *Phys. Rev. Lett.* **56**:1505 (1986).
11. J. Hardy, Y. Pomeau, and O. de Pazzis, *J. Math. Phys.* **14**:1746 (1973).
12. J. L. Lebowitz, E. Orlandi, and E. Presutti, *J. Stat. Phys.* **63**:933 (1991).
13. D. Huse, *Phys. Rev. B* **34**:7485 (1986).
14. M. Rao, M. H. Kalos, J. L. Lebowitz, and J. Marro, *Phys. Rev. B* **13**:4328 (1976).
15. J. L. Lebowitz, J. Marro, and M. H. Kalos, *Comments Solid State Phys.* **10**:201 (1983).
16. J. L. Valles and J. Marro, *J. Stat. Phys.* **49**:89 (1986).
17. J. Marro and J. L. Valles, *J. Stat. Phys.* **49**:121 (1986).
18. J. Marro, P. L. Garrido, A. Labarta, and R. Total, *J. Phys. Condensed Matter* **1**:8147 (1989).
19. K. T. Leung, *Phys. Rev. Lett.* **66**:453 (1991).
20. K. Binder, *Phys. Rev. Lett.* **47**:693 (1981).
21. K. Binder, *Z. Physik* **43**:119 (1981).
22. K. Binder, in *Applications of the Monte Carlo Method in Statistical Physics* (Springer, Berlin, 1984).
23. K. Binder and J. S. Wang, *J. Stat. Phys.* **56**:783 (1989).
24. R. K. Pathria, *Statistical Mechanics* (Pergamon Press, Oxford, 1977).
25. R. Z. P. Zia, Personal communication.